Nanoscale Res Lett (2008) 3:365–371
DOI 10.1007/s11671-008-9168-7

NANO EXPRESS

Synthesis and Visible-Light Photocatalytic Property of Bi_2WO_6 Hierarchical Octahedron-Like Structures

Yuanyuan Li · Jinping Liu · Xintang Huang

Received: 8 August 2008 / Accepted: 2 September 2008 / Published online: 19 September 2008

Abstract A novel octahedron-like hierarchical structure of Bi_2WO_6 has been fabricated by a facile hydrothermal method in high quantity. XRD, SEM, TEM, and HRTEM were used to characterize the product. The results indicated that this kind of Bi_2WO_6 crystals had an average size of ~4 μm, constructed by quasi-square single-crystal nanosheets assembled in a special fashion. The formation of octahedron-like hierarchical structure of Bi_2WO_6 depended crucially on the pH value of the precursor suspensions. The photocatalytic activity of the hierarchical Bi_2WO_6 structures toward RhB degradation under visible light was investigated, and it was found to be significantly better than that of the sample fabricated by SSR. The better photocatalytic property should be strongly associated with the high specific surface area and the abundant pore structure of the hierarchical octahedron-like Bi_2WO_6.

Keywords Nanostructure · Photodegradation · Optical absorption

Introduction

Since the discovery of photoelectrochemical water splitting at a semiconductor surface in 1972, great progress has been made in the research of photocatalytic degradation of organic pollutants for solving environmental problems that confront mankind today. Photocatalysis has many advantages over other treatment methods, for instance, the use of the environmentally friendly oxidant O_2, the easy reaction performed at room temperature, and oxidation of the organic compounds even at low concentrations [1–3]. Much work on photocatalysis in the past decade has focused on TiO_2 for its excellent behaviors in the oxidative degradation of many organic compounds under UV irradiation [4–10]. However, the relatively wide bandgap of 3.2 eV limits its efficient utilization because the UV range is only about 4% of the solar spectrum. In view of the largest proportion of the solar spectrum and artificial light sources, the development of photocatalysts with high activity under a wide range of visible-light irradiation is highly desirable.

There are generally two ways to exploit the photocatalysts responsive to visible-light irradiation: the first involves the modification of TiO_2, and the second is the development of a new photocatalytic material. The former has been extensively investigated by doping with metallic or nonmetallic elements such as V and Cr [11–13] or N [14–18], S [19–21], C [22–24], to gain visible-light response. In contrast, there have been only a few reports on the development of new photocatalyst materials [25–28].

Bi_2WO_6, the simplest member in the Aurivillius family and a potential visible-light photocatalyst, was first studied by Kudo and Hijii [29], Zou's and co-workers [30] groups. Their works revealed that Bi_2WO_6 could perform as an excellent photocatalytic and solar energy transfer material. Photocatalytic activities for O_2 evolution/water splitting and the degradation of the $CHCl_3$ and CH_3CHO under visible-light irradiation were discussed in detail. Encouraged by this progress, various Bi_2WO_6 nanostructures including nanoplates and nanoparticles synthesized by hydrothermal method and their enhanced visible-light-driven photocatalytic activity such as photodegradation of

Y. Li (✉) · J. Liu · X. Huang
Department of Physics, Central China Normal University, Wuhan, 430079 Hubei, People's Republic of China
e-mail: lancyle@mails.ccnu.edu.cn

X. Huang (✉)
e-mail: xthuang@phy.ccnu.edu.cn

rhodamine B(RhB) were reported subsequently [31–35]. On the other hand, spherical superstructures constructed by nano-substructures have been attracting much interest due to their micro/nanostructure and the distinguished physical/chemical properties [36–41]. Large specific surface area and porous structures induced by the hierarchical configuration may improve the contact/interaction between materials and the organic compounds, and thus lead to better photocatalytic performance. As a result, several hierarchical three-dimensional (3D) structures of Bi_2WO_6 [42–44] were also fabricated in the past 2 years.

In a previous work, we fabricated uniform Bi_2WO_6 microspheres governed by a layer-by-layer growth mechanism [44]. We report herein, for the first time, another novel octahedron-like hierarchical structure of Bi_2WO_6 consisting of quasi-square plates joined vertically, and demonstrate its improved visible-light photocatalytic activity in the degradation of RhB as compared to that of the Bi_2WO_6 synthesized by solid-state reaction (SSR). The results indicate that the pH value of precursor suspensions has impact on the morphology of as-prepared products. In addition, the photocatalyst of octahedron-like hierarchically structured Bi_2WO_6 dispersed in alkaline solutions is found to show significantly better photocatalytic ability. Our work will help to develop promising nanostructured photocatalysts that can be more easily separated and recycled.

Experimental

Synthesis of Bi_2WO_6 Hierarchical Octahedron Structures

In a typical procedure, $Bi(NO_3)_3 \cdot 5H_2O$ (2 mmol) was added to 20 mL 1 M HNO_3 to form a clear solution under stirring for 30 min at room temperature. Afterward, 50 mL solution of dissolved 1 mmol $Na_2WO_4 \cdot 2H_2O$ and 0.1 g of PVP was added into the above solution, and a lot of white precipitate appeared quickly. The pH value of the suspension was adjusted to 7 by adding $NH_3 \cdot H_2O$. After constant stirring for another 30 min, the mixture was finally transferred into a 100 mL Teflon-lined autoclave and filled with deionized water up to 80% of the total volume. The autoclave was sealed, maintained at 180 °C for 12 h, and cooled to room temperature naturally. The white precipitate was collected and rinsed several times with distilled water and absolute ethanol, respectively. Then, the sample was dried in a vacuum at 60 °C. For comparison purpose, we also fabricated Bi_2WO_6 by traditional SSR according to Ref. 30 and dispersed nanoplate sample without using PVP.

Characterization

The phase purity of the as-prepared products was determined by X-ray diffraction (XRD Y-2000) with Cu Kα radiation ($\lambda = 1.5418$ Å) at a scan rate of $0.04°s^{-1}$. The morphology of the as-prepared product was characterized by field-emission scanning electron microscopy (FESEM, JEOL, JSM-6700F). Transmission electron microscopy (TEM) was taken with a FEI H-800 transmission electron microscope at an acceleration voltage of 200 kV to further investigate the morphology and structure of Bi_2WO_6 structures. High-resolution transmission electron microscope (HRTEM) images and selected area electron diffraction (SAED) patterns were performed on a JEOL-2010 transmission electron microscope. Room-temperature UV–Vis absorption spectrum was recorded on a UV-1700 spectrophotometer in the wavelength range of 400–800 nm.

Photocatalytic Decomposition of RhB

Photocatalytic activity was evaluated by the degradation of RhB under visible-light irradiation using a 300 W Xe lamp with a cutoff filter ($\lambda > 400$ nm). The reaction cell was placed in a sealed black box, the top of which was open, and the cutoff filter was set on the window face of the reaction cell to ensure the desired irradiation condition. In each experiment, photocatalyst powders (0.5 g/L) were added into RhB solution (1×10^{-5} M, 500 mL). Before illumination, the suspensions were magnetically stirred in the dark for 60 min to ensure the establishment of an adsorption–desorption equilibrium between photocatalyst powders and RhB. At given time intervals, 3 mL suspensions were sampled and centrifuged to remove photocatalyst powders. The filtrates were analyzed by recording the variations of the absorption-band maximum (553 nm) in the UV–Vis spectrum of RhB.

Results and Discussions

Morphology and Structure of Obtained Products

The morphology of the product is shown in Fig. 1. At a low-magnification view in Fig. 1a, many particles with average size of 4 μm are generated in the form of octahedrons. These octahedrons are constructed by three groups of parallel quasi-square plates that are joined vertically (X, Y, and Z directions), as shown in Fig. 1b. An individual octahedron and its enlarged image are illustrated in Fig. 1c and d, respectively. From these pictures, we can observe that several plates of about 20 nm in thickness assemble in an almost parallel fashion and two groups of

the parallel plates are joined vertically to form a cross-like structure; this cross-linked structure can be easily found in every particle from different directions in the low-magnification SEM image. It is noteworthy that plenty of holes are present on the plates, which can typically increase the surface area of the products and enhance the contact area between photocatalyst and organic molecules. The intriguing hierarchical structure of the product can be further interpreted schematically in Fig. 1e. BET surface area is measured to be as much as 26.1 m^2 g^{-1} (from Fig. 2a: N_2 gas adsorption–desorption isotherm), which is much higher than that of the sample obtained by SSR (only $\sim$1.3 m^2 g^{-1} [31]).

The X-ray powder diffraction pattern of the product (Fig. 2b) can be indexed as pure orthorhombic Bi_2WO_6, consistent with the reported data (JCPDS card No. 73-1126, a = 5.457 Å, b = 5.436 Å, c = 16.42 Å). Compared with the standard pattern inserted in Fig. 2b, the intensity ratio of the (200)/(020) peak to the (113) peak increases to 0.61 in the present case, apparently larger than the standard value 0.185, which demonstrates the faster growth of Bi_2WO_6 crystal along the (200)/(020) plane [31].

More information of the structure of the Bi_2WO_6 crystals was obtained by TEM observation (Fig. 3). TEM image of an individual Bi_2WO_6 particle is shown in Fig. 3a. Obviously, the almost square-like outline should be related to the top view of the Bi_2WO_6 octahedron, that is, the projection of a group of parallel plates (can be understood based on Fig. 1e). There is no bright area in the center of the square, quite different from the reported spherical and nest-like Bi_2WO_6 hierarchical structures [42–44], which also means the total thickness of the parallel

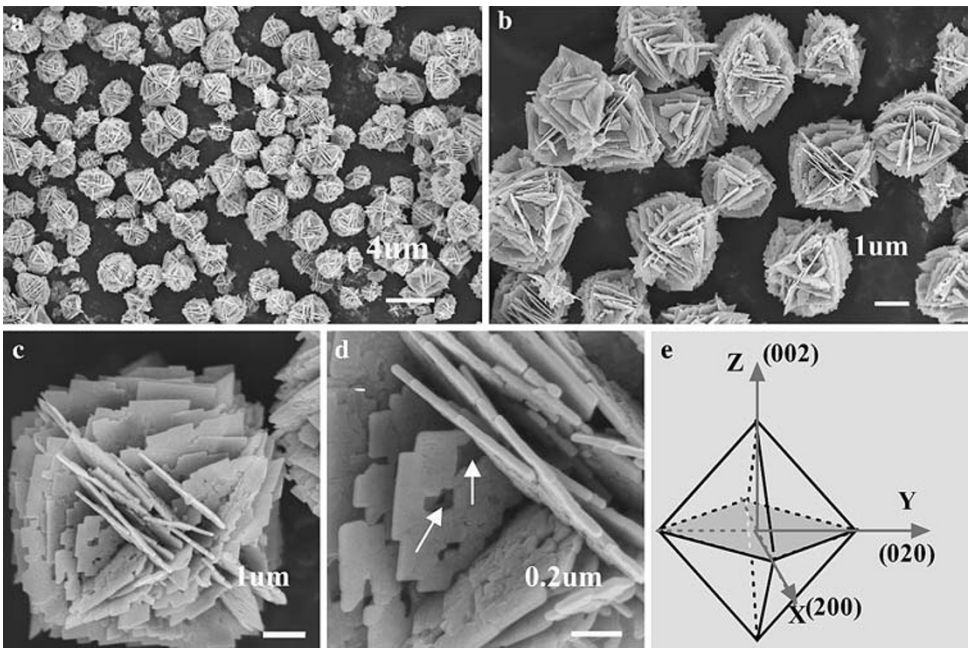

Fig. 1 SEM images of hierarchical Bi_2WO_6 octahedrons: (**a**) low magnification; (**b**) high magnification; (**c**) an individual octahedron; (**d**) enlarged image of **c**; and (**e**) a schematic octahedron structure

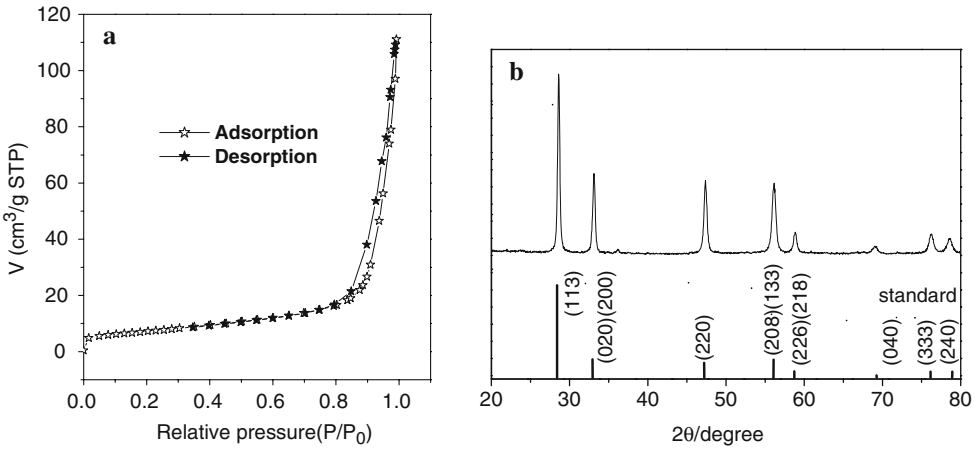

Fig. 2 (**a**) Typical N_2 gas adsorption–desorption isotherm and (**b**) XRD of the as-prepared hierarchical Bi_2WO_6 octahedrons

plates is beyond 100 nm. This is consistent with the above SEM observations that the thickness of a monolayer plate is 20 nm, and naturally the layer number of the parallel plates is above 5. Figure 3b is the SAED pattern of one small plate at the edge of Bi_2WO_6 octahedron. (020) (220) and (200) crystal faces can be easily indexed, and the very uniform spot diffraction pattern implies the single-crystal nature of Bi_2WO_6. High-resolution TEM (HRTEM) image displayed in Fig. 3c reveals a group of clear crystal lattices, and interplanar spacing is measured to be 0.385 nm, corresponding to the (110) plane of orthorhombic Bi_2WO_6. This result also confirms the single-crystal structure of nanoplates.

We found that the pH value of the precursor suspension played a vital role in the Bi_2WO_6 octahedron formation process. Without $NH_3 \cdot H_2O$, the Bi_2WO_6 sample exhibits a uniform 3D sphere-like structure about 4 μm in diameter, as shown in the inset of Fig. 4a. These sphere-like Bi_2WO_6 structures have a dense body consisting of plenty of nanoplates with thickness of 20 nm and length in the range of 100–200 nm (Fig. 4), which were discussed in our previous work. As the amount of $NH_3 \cdot H_2O$ added to the precursor suspension increases, the morphology of the product will change substantially. When the pH value is adjusted to 5.5, the 3D sphere-like Bi_2WO_6 disappears and nonuniform microstructures with several cross-like structures built up by monolayer sheets are present, as shown in the inset of Fig. 4b. With careful observation, some cross-like structures are very similar to the Bi_2WO_6 octahedron, marked by arrowheads in Fig. 4b. Finally, when the pH value reaches 10, only square-like microsized plates with 2 μm in side length can be obtained (Fig. 4c).

As we know, the pH value of the precursor suspension has a strong effect on the hydrolysis of Bi^{3+}, which determines the rates of Bi_2WO_6 nucleation and crystal growth. At low pH value (below 1), the H^+ concentration is much higher than OH^- ion concentration, restraining the hydrolysis of the Bi^{3+}; thus the nucleation rate of Bi_2WO_6 has absolute priority over that of crystal growth. As a

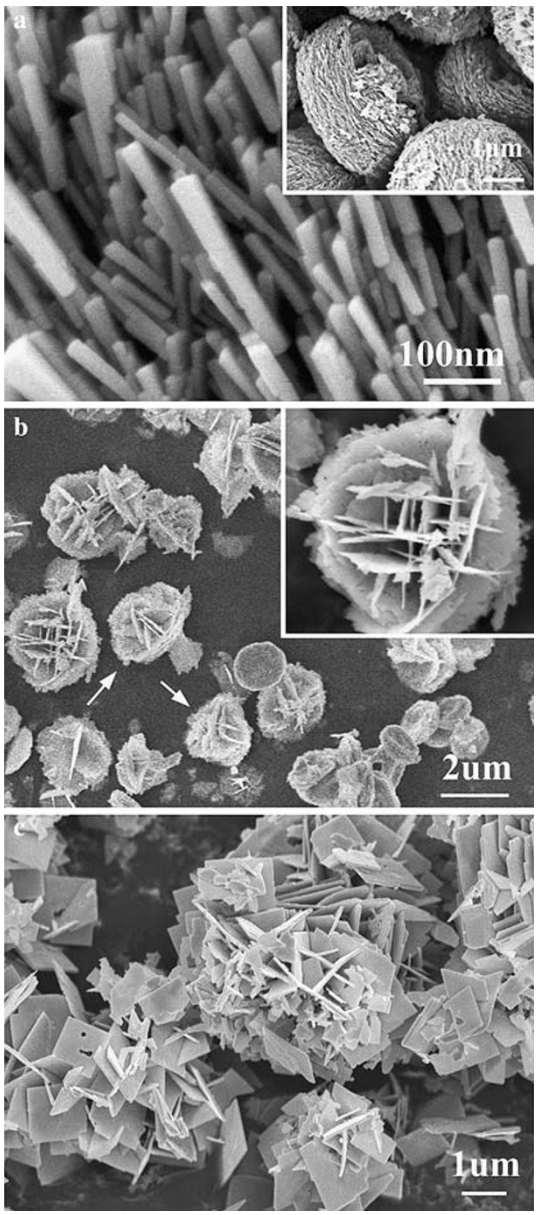

Fig. 4 SEM images of Bi_2WO_6 structures obtained under different pH values (**a**) without $NH_3 \cdot H_2O$; (**b**) pH 5.5; and (**c**) pH 10

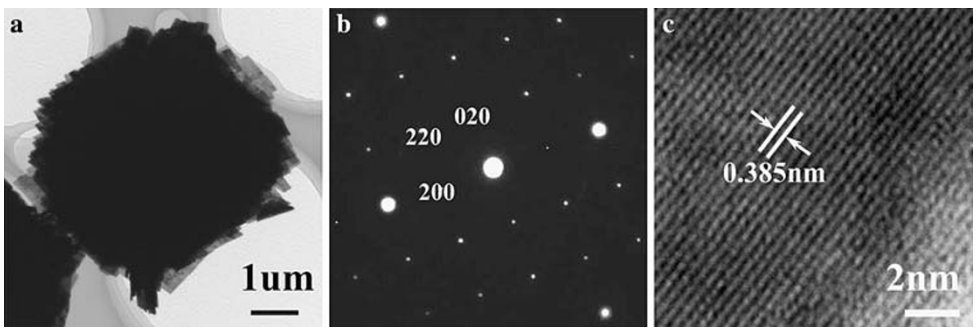

Fig. 3 (**a**) TEM image and (**b**) SAED result of an individual Bi_2WO_6 crystal; (**c**) HRTEM image of the nanoplate at the edge of the octahedron

result, the product is in the form of a microspherical particle constructed by nanoplate subunits according to thermodynamic stability condition (Fig. 4a). The formation of plate-like substructures results from the intrinsic anisotropic layered structure of Bi_2WO_6 [31, 44]. At high pH value (about 10), the rapid hydrolysis of Bi^{3+} decreases the quantity of Bi_2WO_6 nuclei and then the pre-formed seeds have enough resource to contiguously grow and finally form Bi_2WO_6 microplates. In the moderate pH value ($\sim$7), the formation of Bi_2WO_6 nanoplates with appropriate quantity is accompanied by a unique self-assembly process, giving rise to octahedron-like hierarchical structures composed of both parallel and vertical plates. For the assembly of such unique microstructures, the function of PVP and the crystal structure of Bi_2WO_6 material should be considered. Previously, PVP was successfully applied as an important surfactant for the synthesis of various hierarchical nanostructures. In the present work, it was believed that the selective adsorption of PVP on some crystallographic planes of Bi_2WO_6 subunits (small nanoplates) can take place at the initial growth stage. This would help to generate many uniform subunits. As growth time proceeded, the initially formed small plates assembled in an edge-to-edge way with the gradual enlargement of the 2D surfaces. This assembly process greatly lowered the interfacial energy [45] and was facilitated by the square shape of the subunits, which resulted from the crystal structure of Bi_2WO_6. A subsequent layer-by-layer growth of the large nanoplates gave many parallel square plates. Since the formation of parallel plates occurred simultaneously in three dimensions, we could finally observe three groups of parallel square plates cross-linked with (and vertical to) each other, forming octahedron-like structures.

Photocatalytic Activities

The optical property of Bi_2WO_6 hierarchical octahedral structures was measured using UV–Vis spectroscopy, and the result is shown in Fig. 5. It can be seen that the Bi_2WO_6 octahedron has a steep absorption edge in visible range lower than 500 nm, indicating that the absorption relevant to the bandgap is due to the intrinsic transition of the semiconductors. The energy of the bandgap of Bi_2WO_6 hierarchical octahedron estimated from the main absorption edge of the UV–Vis absorption spectrum is $\sim$2.74 eV (inset of Fig. 5), which is suitable for photocatalytic decomposition of organic contaminants under visible-light irradiation.

Next, we study the photocatalytic property of Bi_2WO_6 hierarchical octahedron-like structures. RhB, a widely used dye, was selected to test the degradation efficiency. The major absorption band of RhB is at 553 nm, and the major absorption peaks gradually decrease and shift to shorter

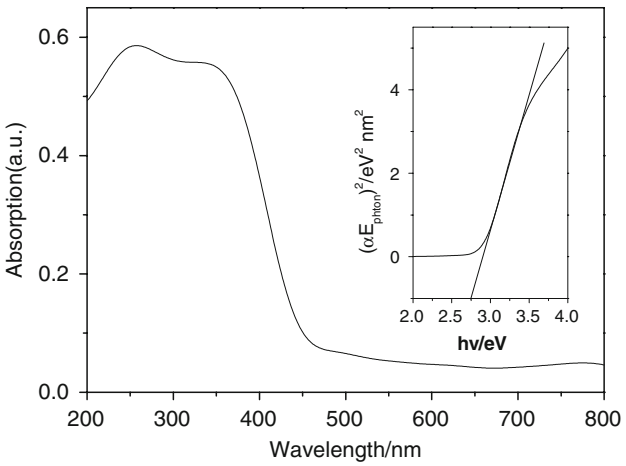

Fig. 5 UV–Vis absorption spectrum of Bi_2WO_6 hierarchical structures. Inset is the plot of $(\alpha E_{photon})^2 \sim E_{photon}$

wavelength step by step as the irradiation time increases [31]. The process of the RhB degradation under visible irradiation is the process of the dye's de-ethylation, that is, from *N*,*N*,*N*′,*N*′-tetraethylated rhodamine to rhodamine. This transition makes the wavelength position of the major absorption peak to move from 553 to 498 nm, as shown in Fig. 6. In addition, the color of dye solution changes from initial red to a light green–yellow, which can be observed by naked eye. The inset of Fig. 6 displays the results of the RhB degradation efficiencies under different conditions. It can be seen that without any photocatalyst (blank) the degradation of RhB is extremely slow, only about 12% after 6 h visible-light irradiation. With Bi_2WO_6 octahedron-like structures dispersed in the RhB solution, the photodegradation of the RhB dye rapidly increases to 56%

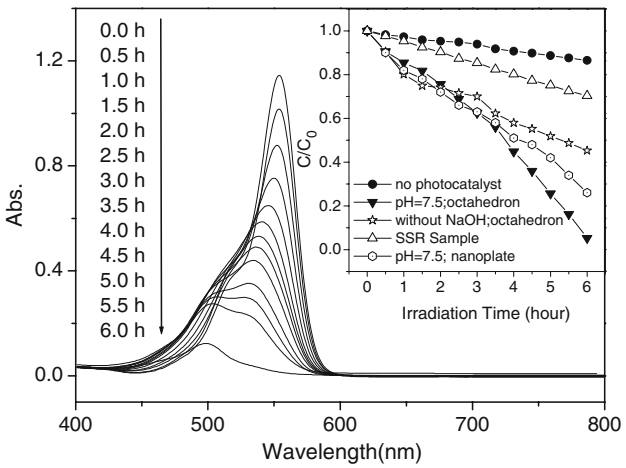

Fig. 6 Absorption spectrum of the RhB solution (1.0×10^{-5} M) in the presence of Bi_2WO_6 octahedron structures under exposure to visible light. The inset shows the photocatalytic performances under different conditions: without photocatalyst; SSR sample; Bi_2WO_6 octahedron structures; Bi_2WO_6 octahedron structures at pH 7.5; and nanoplates at pH 7.5

after the same irradiation time under visible light. pH value of photocatalyst solution is further found to have influence on the photocatalytic ability. When we adjust the pH value of Bi_2WO_6/RhB suspension to 7.5 by adding 5 g/L NaOH aqueous solution, the photodegradation is apparently enhanced: 95% of the RhB can be degraded after 6 h. At pH 7.5 but without photocatalyst, the degradation of RhB is still very slow. It was reported that Bi_2WO_6 photocatalyst directly dispersed in RhB solution is unstable and easy to transform to H_2WO_4 and Bi_2O_3 due to the reaction with H^+ [32]. Thus, the addition of NaOH can help to avoid this side reaction and improve the photocatalytic property.

It is noteworthy that our octahedron-like hierarchical Bi_2WO_6 shows significantly improved photocatalytic activity in comparison with the sample obtained by SSR. As seen from inset of Fig. 6, only 31% of the RhB can be removed after 6-h irradiation when SSR-produced sample is used as the photocatalyst. The reasons accounting for the better photocatalytic activity of our Bi_2WO_6 structures can be explained as follows: (1) photocatalytic process is mainly related to the adsorption and desorption of molecules on the surface of the catalyst. The relatively high specific surface area of the 3D hierarchical structure and a large number of pores in the structure allow more efficient transport of the organic molecules to the active reaction sites, hence enhancing the efficiency of photocatalysis. (2) The high surface-to-volume ratios of nanoplate subunits are beneficial to the separation/transfer of electrons and holes. Due to the laminar structure, holes generated inside the crystals have greater opportunity to transfer to the surface and act with the RhB. Indeed, as shown in the inset of Fig. 6, nanoplates exhibit much better catalytic ability than SSR sample. (3) Porous appearance in the octahedron-like hierarchical structures may also enhance visible-light transmission and utilization. It should be further pointed out that the 3D hierarchical structures can be readily dispersed due to the micrometer size, avoiding the unwanted aggregations (this exists in nanoplate sample) during the photocatalytic process. Also, the larger size will facilitate the separation and recycling of photocatalysts, which is very important for environmental application.

Conclusions

In this paper, we report the hydrothermal synthesis of a novel hierarchical octahedron-like structure of Bi_2WO_6, which has an average size of $\sim$4 μm and consists of many quasi-square nanosheets. The effect of pH value of the precursor suspensions on the formation of octahedron-like Bi_2WO_6 crystals is discussed. Importantly, as a potential visible-light photocatalyst, our octahedron-like Bi_2WO_6 exhibits much better activity for the photodegradation of RhB as compared to the photocatalyst product fabricated by SSR.

References

1. X. Tao, W. Ma, T. Zhang, J. Zhao, Angew. Chem. Int. Ed. **40**, 3014 (2001). doi:10.1002/1521-3773(20010817)40:16<3014::AID-ANIE3014>3.0.CO;2-M
2. W. Ma, J. Li, X. Tao, J. He, Y. Xu, J.C. Yu et al., Angew. Chem. Int. Ed. **42**, 1029 (2003). doi:10.1002/anie.200390264
3. J.L. Falconer, K.A. Magrini-Bair, J. Catal. **179**, 171 (1998). doi:10.1006/jcat.1998.2215
4. J.M. Herrmann, J. Disdier, P. Pichat, J. Catal. **113**, 72 (1988). doi:10.1016/0021-9517(88)90238-2
5. D.S. Muggli, J.T. McCue, J.L. Falconer, J. Catal. **173**, 470 (1998). doi:10.1006/jcat.1997.1946
6. X.Z. Li, F.B. Li, Environ. Sci. Technol. **35**, 2381 (2001). doi:10.1021/es001752w
7. D.S. Muggli, L. Ding, M.J. Odland, Catal. Lett. **78**, 23 (2002). doi:10.1023/A:1014954114655
8. J. Fernandez, J. Kiwi, C. Lizama, J. Freer, J. Baeza, H.D. Mansilla, J. Photochem. Photobiol. A **151**, 213 (2002). doi:10.1016/S1010-6030(02)00153-3
9. A.A. Belhekar, S.V. Awate, R. Anand, Catal. Commun. **3**, 453 (2002). doi:10.1016/S1566-7367(02)00179-6
10. T. Tsumura, N. Kojitan, I. Izumi, N. Iwashita, M. Toyoda, M. Inagaki, J. Mater. Chem. **12**, 1391 (2002). doi:10.1039/b201942f
11. E. Borgarello, J. Kiwi, M. Gratzel, E. Pelizzetti, M. Visca, J. Am. Chem. Soc. **104**, 2996 (1982). doi:10.1021/ja00375a010
12. N. Serpone, D. Lawless, J. Disdier, J.M. Herrmann, Langmuir **10**, 643 (1994). doi:10.1021/la00015a010
13. H. Yamashita, M. Harada, J. Misaka, M. Takeuchi, K. Ikeue, M. Anpo, J. Photochem. Photobiol. A **148**, 257 (2002). doi:10.1016/S1010-6030(02)00051-5
14. S. Sato, Chem. Phys. Lett. **123**, 126 (1986). doi:10.1016/0009-2614(86)87026-9
15. R. Asahi, T. Morikawa, T. Ohwaki, K. Aoki, Y. Taga, Science **293**, 269 (2001). doi:10.1126/science.1061051
16. T. Morikawa, R. Asahi, T. Ohwaki, K. Aoki, Y. Taga, Jpn. J. Appl. Phys. **40**, 561 (2001). doi:10.1143/JJAP.40.L561
17. S. Sakthivel, H. Kisch, ChemPhysChem. **4**, 487 (2003). doi:10.1002/cphc.200200554
18. H. Irie, Y. Watanabe, K. Hashimoto, J. Phys. Chem. B **107**, 5483 (2003). doi:10.1021/jp030133h
19. T. Umebayashi, T. Yamaki, H. Itoh, K. Asai, Appl. Phys. Lett. **81**, 454 (2002). doi:10.1063/1.1493647
20. T. Umebayashi, T. Yamaki, S. Tanaka, K. Asai, Chem. Lett. **32**, 330 (2003). doi:10.1246/cl.2003.330
21. T. Ohno, T. Mitsui, M. Matsumura, Chem. Lett. **32**, 364 (2003). doi:10.1246/cl.2003.364
22. C. Lettmann, K. Hildenbrand, H. Kisch, W. Macyk, W.F. Maier, Appl. Catal. B **32**, 215 (2001). doi:10.1016/S0926-3373(01)00141-2
23. S.U.M. Khan, M. Al-Shahry, W.B. Ingler, Science **297**, 2243 (2002). doi:10.1126/science.1075035
24. S. Sakthivel, H. Kisch, Angew. Chem. Int. Ed. **42**, 4908 (2003). doi:10.1002/anie.200351577
25. H.B. Lu, H. Li, L. Liao, Y. Tian, M. Shuai, J.C. Li et al., Nanotechnology **19**, 045605 (2008). doi:10.1088/0957-4484/19/04/045605
26. H.G. Kim, D.W. Hwang, J.S. Lee, J. Am. Chem. Soc. **126**, 8912 (2004). doi:10.1021/ja049676a

27. H.B. Zeng, W.P. Cai, P.S. Liu, X.X. Xu, H.J. Zhou, C. Klingshirn, H. Kalt, ACS Nano. (2008). doi:10.1021/nn800353q
28. H. Kato, H. Kobayashi, A. Kudo, J. Phys. Chem. B **106**, 12441 (2002). doi:10.1021/jp025974n
29. A. Kudo, S. Hijii, Chem. Lett **10**, 1103 (1999). doi:10.1246/cl.1999.1103
30. J.W. Tang, Z.G. Zou, J.H. Ye, Catal. Lett. **92**, 53 (2004). doi:10.1023/B:CATL.0000011086.20412.aa
31. C. Zhang, Y. Zhu, Chem. Mater. **17**, 3537 (2005). doi:10.1021/cm0501517
32. H. Fu, C. Pan, W. Yao, Y. Zhu, J. Phys. Chem. B **109**, 22432 (2005). doi:10.1021/jp052995j
33. S. Zhang, C. Zhang, Y. Man, Y.F. Zhu, J. Solid State Chem. **179**, 62 (2005). doi:10.1016/j.jssc.2005.09.041
34. H.B. Fu, L.W. Zhang, W.Q. Yao, Y.F. Zhu, Appl. Catal. B **66**, 100 (2006). doi:10.1016/j.apcatb.2006.02.022
35. J.G. Yu, J.F. Xiong, B. Cheng, Y. Yu, J.B. Wang, J. Solid State Chem. **178**, 1968 (2005). doi:10.1016/j.jssc.2005.04.003
36. J.H. Jung, Y. Ono, K. Sakurai, M. Sano, S. Shinkai, J. Am. Chem. Soc. **122**, 8648 (2000). doi:10.1021/ja001623f
37. S. Park, J.H. Lim, S.W. Chung, C.A. Mirkin, Science **303**, 348 (2004). doi:10.1126/science.1093276
38. T.D. Ewers, A.K. Sra, B.C. Norris, R.E. Cable, C.H. Cheng, D.F. Shantz et al., Chem. Mater. **17**, 514 (2005). doi:10.1021/cm0483792
39. H.T. Zhang, X.H. Chen, J. Phys. Chem. B **110**, 9442 (2006). doi:10.1021/jp061088r
40. M.W. Heaven, G.W.V. Cave, R.M. McKinlay, J. Antesberger, S.J. Dalgarno, P.K. Thallapally et al., Angew. Chem. Int. Ed. **45**, 6221 (2006). doi:10.1002/anie.200600671
41. J.N.H. Reek, M.J. Crossley, A.P.H.J. Schenning, A.W. Bosman, E.W. Meijer, Chem. Commun. (Camb.) **1**, 11 (1998). doi:10.1039/a707748c
42. L.S. Zhang, W.Z. Wang, Z.G. Chen, L. Zhou, H.L. Xu, W. Zhu, J. Mater. Chem. **17**, 2526 (2007). doi:10.1039/b616460a
43. J. Wu, F. Duan, Y. Zheng, Y. Xie, J. Phys. Chem. C **111**, 12866 (2007). doi:10.1021/jp073877u
44. Y.Y. Li, J.P. Liu, X.T. Huang, G.L. Li, Cryst. Growth Des. **7**, 1350 (2007). doi:10.1021/cg070343+
45. J.P. Liu, X.T. Huang, Y.Y. Li, Z.K. Li, J. Mater. Chem. **17**, 2754 (2007). doi:10.1039/b703552g